Chong-Won Lee
Yun-Sik Han
Center for Noise and Vibration Control (NOVIC)
Department of Mechanical Engineering
Korea Advanced Institute of Science and Technology
Science Town, Taejon 305-701
South Korea

Jong-Po Park
Vibration Research Team
Research and Development Center
Korea Heavy Industries and Construction Co., Ltd.
P.O. Box 77, Changwon 641-792
South Korea

Use of Directional Spectra for Detection of Engine Cylinder Power Fault

A diagnostic method, which uses the two-sided directional power spectra of complex-valued engine vibration signals, is presented and tested with four-cylinder compression and spark ignition engines for the diagnosis of cylinder power faults. As spectral estimators, the maximum likelihood and FFT methods are compared, and the multi-layer neural network is employed for pattern recognition. Experimental results show that the success rate for identifying the misfired cylinder is much higher with the use of two-sided directional power spectra than conventional one-sided power spectra.

INTRODUCTION

As the stringent regulatory requirements on the reduction of exhaust gas emissions are imposed, the detection and the isolation of misfired cylinder in the automotive engine become increasingly important. A direct method for detecting a misfired engine cylinder is to measure the cylinder pressure. However, this is not practical because it is difficult to insert pressure sensors inside all cylinders. This leads to the development of indirect methods among most of the investigators in this area. Signature analysis of fluctuations of crankshaft speed presented by Rizzoni (1989), Connolly and Yagle (1993), used the instantaneous angular velocity of an engine flywheel as a diagnostic tool for engine. But this method requires setting up an additional equipment to measure torsional velocity variation, and using a trigger pulse signal. Kim and Lyon (1992) proposed a high level diagnostic method, utilizing cepstral analysis to extract the robust transfer function and then to identify the cylinder pressure from measurement of engine block vibrations. It requires the pressure signal of a cylinder and can be applied to the same kind of engines. But a reference trigger signal was required for detecting a misfired cylinder.

Received 18 March 1997; Revised 16 September 1997.
Shock and Vibration, Vol. 4, No. 5,6, pp. 391–401 (1997)
ISSN 1070-9622/97/$8.00

To diagnose defective elements in a structure or machine, signature analysis is necessary to extract some important features which describe the condition of each element. Spectral analysis is probably the most popular signal processing technique for diagnosing mechanical failures or faults because the frequency components and the corresponding amplitudes vary in accordance with various fault mechanisms. In particular, the *directional* power spectra (dPS) of complex-valued signals have proven to be a diagnostic tool for rotating machinery (Lee, 1991; Lee, 1993; Lee and Joh, 1994a; Lee and Joh, 1994b). However, the dPS technique, originally developed for rotating machinery, can also be applied to nonrotating machines, as will be shown in this paper.

In this work, complex-valued vibration signals measured from an engine block are used to acquire some important features of its motion in space. As a spectral estimator, the FFT method has inherent limitations related to frequency resolution, variability, and inability to discern between narrow-band random and true periodic components, while the Autoregressive (AR) and Maximum Likelihood (ML) spectral estimators possess better capabilities in frequency resolution and power estimates, respectively (Sherman, 1991). In this paper, the *directional* AR and ML spectral estimators are introduced to accommodate *complex*-valued signals, the resulting dPS are used for diagnosis of engine cylinder power faults, and the results are compared with the conventional FFT method. Furthermore, the diagnostic technique used in this work is fully compared with the one that uses the conventional one-sided PS.

For the automatic detection/diagnosis of cylinder power faults, a pattern recognition method using the multi-layer neural networks is employed.

DIRECTIONAL POWER SPECTRUM

Recently, use of dPS has been proposed for effective identification and diagnosis of rotating machinery (Lee, 1991; Lee, 1993; Lee and Joh, 1994a; Lee and Joh, 1994b; Park and Lee, 1995). The key idea is that, in general, a planar whirling motion of a rotor in operation can be decomposed into *backward* (the direction opposite to the rotor rotation) and *forward* (the same direction as the rotor rotation) harmonic components. The harmonic components, backward or forward, can be directly identified in the directional spectrum which is acquired from the Fourier transform of the complex-valued signal representing planar motion of the rotor. The complex-valued signal is usually made up of two

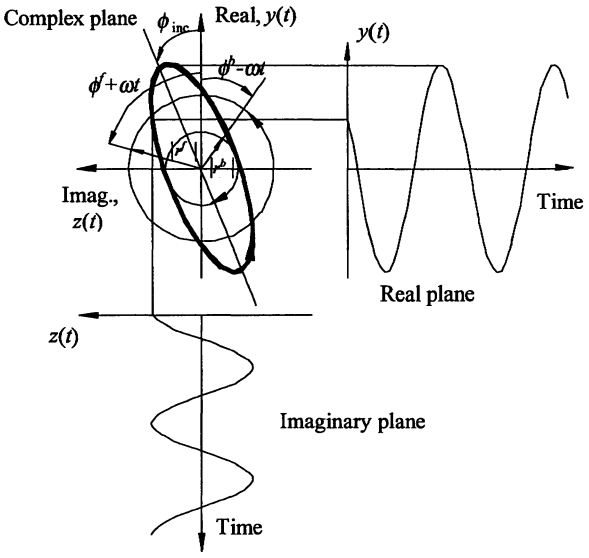

FIGURE 1 Representation of a complex-valued signal as the sum of two contra-rotating vectors.

real-valued signals measured from two vibration transducers, placed perpendicular to each other. The positive (negative) frequency components appearing in the dPS physically correspond to forward (backward) *whirling* components. Thus the variations in forward and backward frequency components of dPS can be effectively used for diagnosing any defects or faults in a rotating machine, which cause the change in whirl orbits or Lissajous figures.

The same idea can also be applied to nonrotating vibratory machines. A point of interest on a machine in operation will generally vibrate in three-dimensional space, making a complicated trajectory. The projected trajectory on an arbitrary plane, resembling a whirl orbit, can then be treated in a similar way to a whirling motion of a rotor. Let us first consider a complex signal $p(t) = y(t) + \mathrm{j}z(t)$ by using a complex notation for the projected planar motion. Here, $y(t)$ and $z(t)$ are the real signals, j $(= \sqrt{-1})$ denotes the imaginary number. It is then natural to associate the complex signal $p(t)$ with a moving point, or a moving vector drawn from the origin, in the plane whose Cartesian coordinates are $y(t)$ and $z(t)$. When we try to display the complex signal $p(t)$ geometrically in the complex plane, the y-axis becomes the real axis, the z-axis being the imaginary axis, as indicated in Fig. 1. The complex harmonic signal $p(t)$ of frequency ω can be rewritten in polar form, using Euler's formula, as

$$\begin{aligned} p(t) &= y(t) + \mathrm{j}z(t) = p^f(t) + p^b(t) \\ &= r^f e^{\mathrm{j}\omega t} + r^b e^{-\mathrm{j}\omega t} \\ &= \left\{ \frac{1}{2}(y_c + z_s) + \frac{\mathrm{j}}{2}(z_c - y_s) \right\} e^{\mathrm{j}\omega t} \end{aligned}$$

$$+\left\{\frac{1}{2}(y_c - z_s) + \frac{\mathrm{j}}{2}(z_c + y_s)\right\}e^{-\mathrm{j}\omega t}, \quad (1)$$

where, $p^f(t) = r^f e^{\mathrm{j}\omega t}$, $p^b(t) = r^b e^{-\mathrm{j}\omega t}$, $y(t) = y_c \cos\omega t + y_s \sin\omega t$, $z(t) = z_c \cos\omega t + z_s \sin\omega t$, $r^f = |r^f|e^{\mathrm{j}\phi^f}$, $r^b = |r^b|e^{\mathrm{j}\phi^b}$. Here the superscripts b and f denote the backward (clockwise) and forward (counter-clockwise in Fig. 1) components, and, y_c and y_s (z_c and z_s) are the Fourier coefficients associated with $y(t)$ ($z(t)$). Note that the complex term $e^{\mathrm{j}\omega t}$ ($e^{-\mathrm{j}\omega t}$) is associated with the forward (backward) rotating unity vector at the circular rotating speed of ω and that the complex quantity r^f (r^b) is associated with the vector having the amplitude, $|r^f|$ ($|r^b|$), and the initial phase, ϕ^f (ϕ^b). It is well known that the complex harmonic signal, which is the resultant of two contra-rotating vectors, each with different amplitudes and initial phases, forms an ellipse in the complex plane. The shape and directivity of the elliptic planar motion are determined as follows:

$$\begin{aligned}
&r^f\,(r^b) = 0 \;:\; \text{backward (forward) circular planar motion,}\\
&|r^b| > |r^f| \;:\; \text{backward elliptic planar motion,}\\
&|r^b| = |r^f| \;:\; \text{straight line motion,}\\
&|r^b| < |r^f| \;:\; \text{forward elliptic planar motion.}
\end{aligned} \quad (2)$$

Note that the power spectral components at the frequencies $-\omega_k$ and ω_k are equal to $|r_k^b|^2$ and $|r_k^f|^2$, respectively. The directional spectral density functions of a complex-valued signal $p(t)$ are defined in terms of the conventional spectral density functions, as

$$\begin{aligned}
P_{pp}(\omega) &= P_{yy}(\omega) + P_{zz}(\omega) + \mathrm{j}\big(P_{yz}(\omega) - P_{zy}(\omega)\big)\\
&= P_{yy}(\omega) + P_{zz}(\omega) - 2\cdot \mathrm{Im}\big\{P_{yz}(\omega)\big\}.
\end{aligned} \quad (3)$$

Here, the quantity $P_{pp}(\omega)$ is called the directional power spectral density function (dPSD). For the real random signals, the spectral density functions satisfy such symmetric properties as

$$\begin{aligned}
P_{yy}(-\omega) &= \overline{P}_{yy}(\omega) = P_{yy}(\omega),\\
P_{yz}(-\omega) &= \overline{P}_{yz}(\omega) = P_{zy}(\omega)
\end{aligned} \quad (4)$$

which implies that the conventional PSD, $P_{yy}(\omega)$, is a real, even function of ω. Thus, the directional spectra satisfy

$$P_{pp}(-\omega) = P_{\overline{pp}}(\omega) \quad (5)$$

which suggests that the dPSD, $P_{pp}(\omega)$, of a complex signal is a real, but not necessarily even function of ω. And, the dPSD has the nonnegative property, that is,

$$P_{pp}(\omega) \geqslant 0. \quad (6)$$

Note that the dPSD defined in Eq. (3) gives not only frequency content but also directivity and shape of the planar motion, unlike the conventional PSD which only gives one-sided frequency content. In this way, the dPSD contains richer information regarding the planar motion than the PSD.

In this paper, the dPSD technique is introduced for diagnosis of two automobile engines, typical nonrotating machines.

PROPERTIES OF AR AND ML SPECTRA

It is well known (Capon, 1969; Lacoss, 1971; Kay, 1988) that the dPS estimate of an observation process by the ML method, can be expressed as

$$P_{\mathrm{ML}}^n(f) = \frac{1}{\mathbf{e}^{\mathrm{H}}\mathbf{R}_{nn}^{-1}\mathbf{e}}, \quad (7)$$

where $\mathbf{e}$ is the complex sinusoid vector given by

$$\mathbf{e} = \left\{1 \;\exp(\mathrm{j}2\pi f h) \;\ldots\; \exp\big(\mathrm{j}2\pi f(n-1)h\big)\right\}',$$

Here $\mathbf{R}_{nn}^{-1}$ is the inverse of the $n \times n$ estimated *complex* autocorrelation matrix, the prime and superscript H denote the transpose and Hermitian, respectively, and h is the equi-spaced sampling interval. The relationship between ML power spectrum and AR power spectral densities (PSD) is given as (Burg, 1972; Kay, 1988)

$$\frac{1}{P_{\mathrm{ML}}^n(f)} = \sum_{i=1}^{n} \frac{1}{S_{\mathrm{AR}}^i(f)}, \quad (8)$$

$$S_{\mathrm{AR}}^i(f) = \frac{h\sigma_\varepsilon^2}{\left|1 - \sum_{m=1}^{i} \phi_m \exp(\mathrm{j}2\pi f m h)\right|^2}, \quad -\frac{1}{2h} \leqslant f \leqslant \frac{1}{2h} \quad (9)$$

where the superscript i denotes the AR order, ϕ_m are the *complex* AR coefficients and the σ_ε^2 is the variance of noise. The low frequency resolution of the ML is due to the "parallel resistor network averaging" of the lowest to the highest resolution AR spectra.

The asymptotic behaviors of the AR and ML estimates are given as (Foias et al., 1989; Kay, 1988)

$$\begin{aligned}
\lim_{i\to\infty} S_{\mathrm{AR}}^i(f) &= \begin{cases} \infty, & \text{at } f = f_k,\\ S_\varepsilon(f), & \text{otherwise,}\end{cases}\\
\lim_{n\to\infty} P_{\mathrm{ML}}^n(f) &= \begin{cases} |A_k^f|^2, & \text{at } f = f_k,\\ 0, & \text{otherwise,}\end{cases}
\end{aligned} \quad (10)$$

where $S_\varepsilon(f)$ denotes the complex noise PSD. According to Eq. (9), in any regular noise environment and

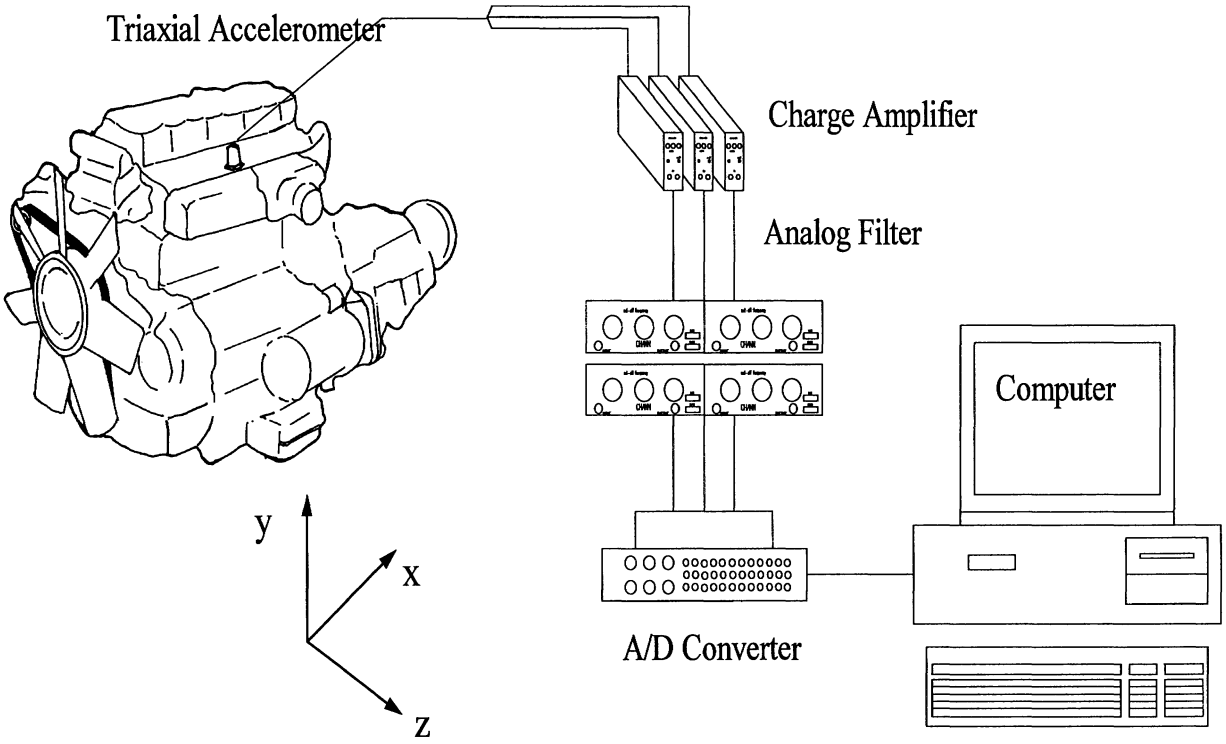

FIGURE 2 Experimental setup and coordinate system.

for any signal-to-noise ratio, the sequence of ML estimates converges monotonically either to zero if the frequency does not correspond to a sinusoid, or to the power of the sinusoid if it does. Thus it provides signal amplitude and frequency information simultaneously. Practically all spectral estimation methods, including the very popular FFT- and AR-based approaches, suffer from the problem that for a finite value of correlation lag there is no natural rule for deciding which peaks correspond to sinusoids and which do not. Hence, they usually assume that the highest spectral peaks correspond to the point spectrum. The monotonic convergence of the ML estimate in (10) provides a natural rule for detecting and estimating point spectra using a finite number n (Sherman and Lou, 1989). Equation (10) implies that it is generally impossible to extract signal amplitude information directly from the AR spectral estimate; for sufficiently well behaved noise, it may be possible to obtain a reliable power spectral estimate for a sinusoid with a known frequency by calculating the area under the power spectral density peak (Lacoss, 1971; Kay, 1988). The AR power spectral density estimates $S^i_{\mathrm{AR}}(f)$ can be used as a good frequency detector for point spectra.

In this work, the conventional AR and ML estimators are extended to accommodate complex-valued signals and adopted as frequency and power detectors, respectively.

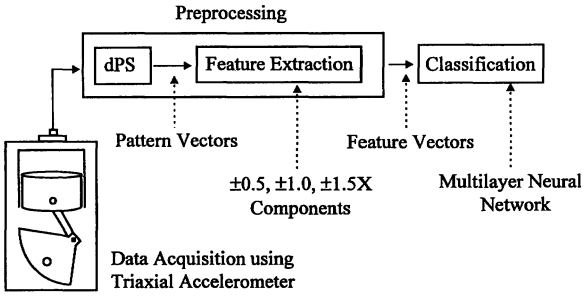

FIGURE 3 Schematic diagram of diagnosis procedures.

EXPERIMENT

Experimental Set-up

Experiments were carried out using the following two setups: one was a four-stroke four-cylinder inline compression ignition engine on three-point engine mounts, mounted on a test stand in the laboratory, and the other was a four-stroke four-cylinder inline spark ignition engine, mounted in a vehicle. To simulate the misfiring in a cylinder of the compression ignition engine, the fuel line to the cylinder was disconnected when the engine was idling. In the vehicle equipped with the spark ignition engine, the electric wiring connected with a spark ignition plug was taken

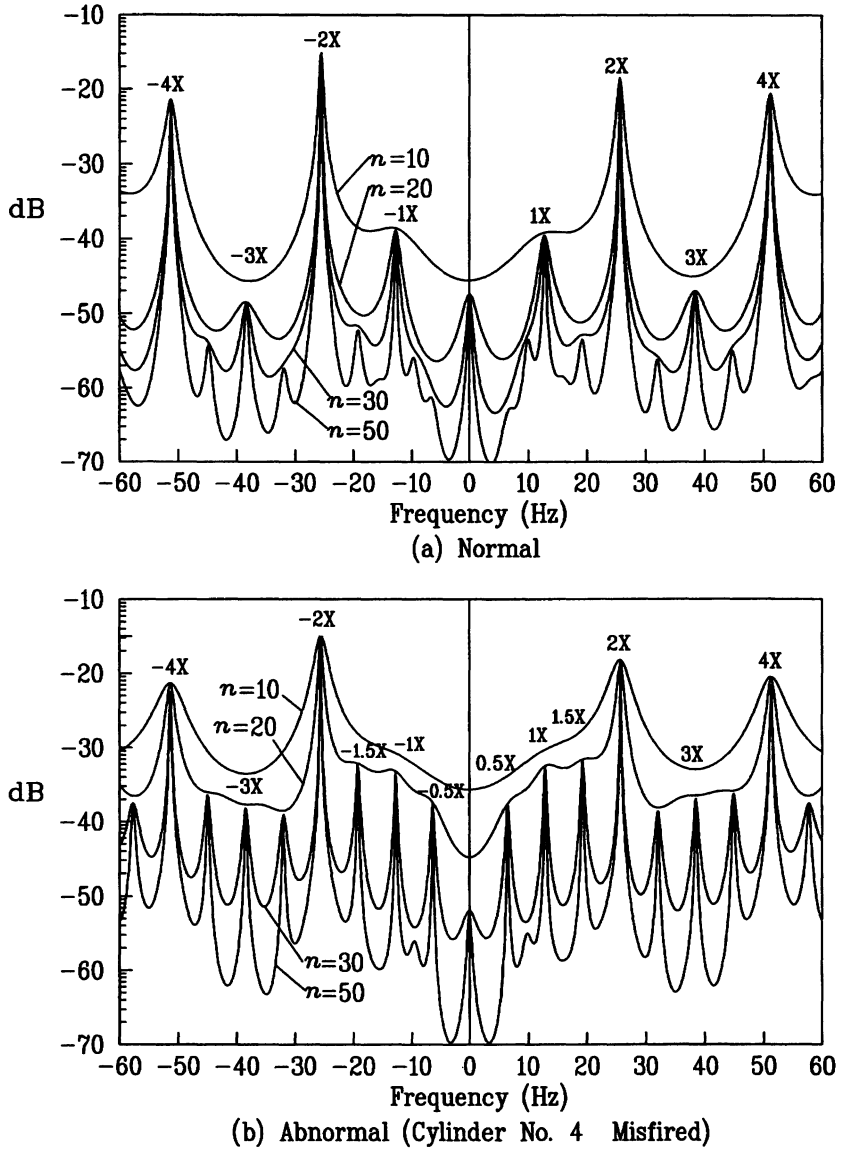

FIGURE 4 Typical ML dPSs of engine vibration: compression ignition engine. (a) normal, (b) abnormal (cylinder No. 4 misfired).

out in an idling speed. A triaxial accelerometer positioned at the midpoint of the top of the engine block was used to measure the vibrations in the three perpendicular directions x, y and z, as shown in Fig. 2. The vibration signals were low-pass filtered to prevent aliasing and subsequently sampled at a rate of 140 Hz by a 12-bit A/D converter. The sampled data sequences were saved in a personal computer for the directional spectral analysis. In the compression (spark) ignition engine, thirty (ten) data sets were obtained under both normal and abnormal engine conditions, where each data set consisted of 1024 data points. Throughout the experiments, the compression (spark) ignition engine speed was held to about 770 (1500) rpm with no loading.

With the measurements in the x, y, and z directions, we can define three different planar motions, one of which can always be regenerated from the other two. For convenience, we will only deal with the frontal planar motion by introducing the complex-valued signal $p(t) = y(t) + jz(t)$. Figure 3 shows the schematic diagram of signal processing procedures employed for detection of a misfired engine cylinder. Considering a normal four-stroke four-cylinder engine with ignition interval T, the complex-valued vibration signal measured from the engine block can be treated as a periodic function with period $T(\equiv \frac{1}{f_n})$. Thus, the ma-

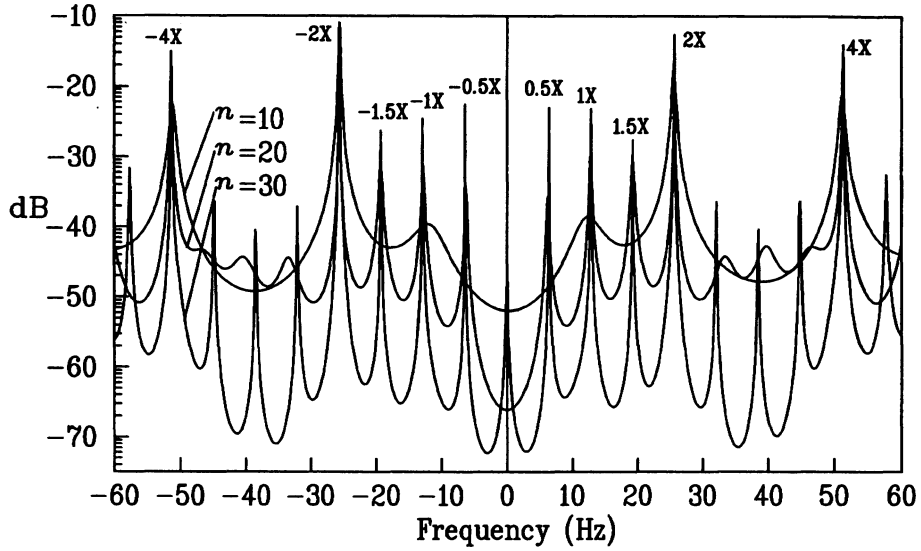

FIGURE 5 Typical AR dPSD of engine vibration: compression ignition engine with cylinder No. 4 misfired.

jor peaks in the dPS of the vibration signals appear at frequencies $\pm kf_n$, $k = 1, 2, \ldots$ Similarly, considering an abnormal engine with a misfired cylinder, a complex-valued vibration signal can be treated as a periodic function with period $4T$ ($f_a \equiv \frac{1}{4T} = 0.5X$; $1X$ = crankshaft rotation frequency), and the amplitudes of these fractional order terms are affected more dramatically than the integer order terms. Thus, we intended to utilize the six frequencies components, $\pm\frac{f_n}{4}$ ($\pm 0.5X$), $\pm\frac{2f_n}{4}$ ($\pm 1X$) and $\pm\frac{3f_n}{4}$ ($\pm 1.5X$) for pattern classifications by neural networks as shown in Fig. 3.

RESULTS AND DISCUSSION

Figure 4 shows the typical ML dPS of the acceleration signals measured under the normal and abnormal engine conditions. Note that the $\pm 0.5X$, $\pm 1X$ and $\pm 1.5X$ components become significant for the abnormal engine condition as expected, and that it is required to have at least $n = 30$ for adequate spectral estimates. Figure 5 shows the typical AR dPSD estimate, which indicates that its frequency resolving property is far superior to the ML spectrum (Sherman and Lou, 1989). However, the peaks of the AR dPSD at the corresponding frequencies exhibit no consistent trend as n increases, because it is a density function estimate.

Figure 6 shows the typical trajectory of the measurement point on the engine block with cylinder no. 3 misfired and the orbits of the harmonic components associated with $\pm 0.5X$, $\pm 1X$ and $\pm 1.5X$.

Figures 7 and 8 show the normalized power spectral estimates, at the frequencies of interest, obtained by the FFT and ML methods, respectively, where 30 data sets are used for calculations of means and standard deviations. Because the data sets have been measured in enough time intervals, the power spectral estimates have some derivations. The power spectral estimate at a frequency of interest by the FFT method was obtained by calculating the area under the corresponding spectral peak, while the peak value of the ML dPS estimate itself at a frequency directly corresponds to power. Deviation in the dPS estimates by FFT is found to be slightly larger than that by ML as shown in Tables 1 and 2. Note that the dPS with cylinder no. 1 or 4 misfired is clearly distinguishable from the dPS with cylinder no. 2 or 3 misfired by comparing $\pm 1X$ components, and the dPS with cylinder no. 2 (no. 1) misfired differs particularly in $\pm 1.5X$ ($\pm 1X$ and $\pm 1.5X$) components from that with cylinder no. 3 (no. 4) misfired.

For the automatic detection/diagnosis of cylinder power faults, a pattern recognition method using the multi-layer neural network shown in Fig. 9 is employed (Pao, 1989). The neural network is composed of the input layer with six nodes, the output layer with five nodes, which are due to the six frequency components of interest and the five patterns, i.e., the normal and four abnormal patterns, and the hidden layer with five nodes. The generalized delta rule, so-called the error back-propagation algorithm, is used as learning algorithm of the neural network. The change in connection weights for the generalized delta rule is re-

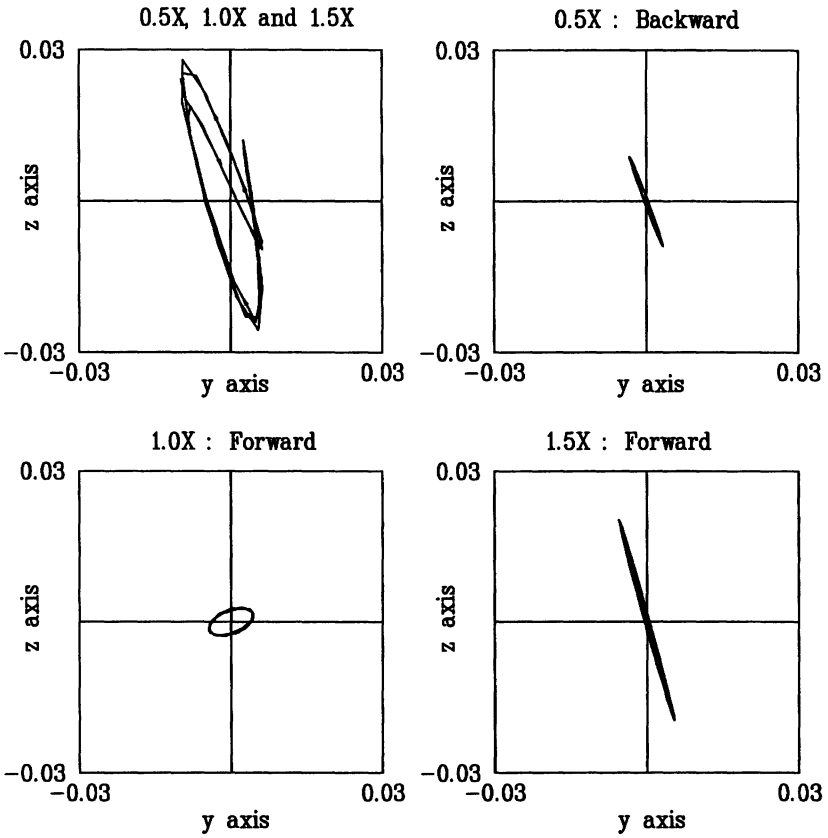

FIGURE 6 Trajectory of measurement point on engine block: compression ignition engine with cylinder No. 3 misfired.

Table 1. Normalized Means of dPS Estimates by FFT: Compression Ignition Engine at 770 rpm

Conditions	Normalized Means of Power Estimates						Avg. of Dev.(%)[3]
	$-1.5x$	$-1.0x$	$-0.5x$	$0.5x$	$1.0x$	$1.5x$	
Normal	0.044(51.)[2]	0.142(8.4)	0.006(77.)	0.005(81.)	0.120(5.7)	0.025(48.)	(45.7)
Cyl. # 1[1]	0.857(12.)	0.459(9.9)	0.151(7.3)	0.145(8.6)	0.550(18.)	0.861(11.)	(11.5)
Cyl. # 2	0.827(15.)	0.019(34.)	0.173(14.)	0.172(14.)	0.155(7.8)	0.860(16.)	(17.3)
Cyl. # 3	**1.000**(9.4)	0.026(44.)	0.189(7.7)	0.170(8.5)	0.094(18.)	0.994(7.8)	(16.0)
Cyl. # 4	0.667(5.8)	0.510(4.3)	0.166(11.)	0.161(12.)	0.609(5.6)	0.729(4.8)	(7.42)

Note: (1) Misfired Cylinder No., (2) S_i = Standard Deviation/Mean × 100%, (3) $\overline{S}_i = \frac{1}{6}\sum_{i=1}^{6} S_i$
Average of Total Dev.(Excluding Normal) = $\frac{1}{5(4)}\sum_{i=1}^{5(4)} \overline{S}_i$ = **19.6%** (**13%**), Datapoints Used = **1024**

Table 2. Normalized Means of dPS Estimates by ML: Compression Ignition Engine at 770 rpm

Conditions	Normalized Means of Power Estimates						Avg. of Dev.(%)
	$-1.5x$	$-1.0x$	$-0.5x$	$0.5x$	$1.0x$	$1.5x$	
Normal	0.012(49.)	0.014(4.0)	0.003(34.)	0.002(41.)	0.118(7.2)	0.011(54.)	(32.0)
Cyl. # 1	0.831(12.)	0.449(9.3)	0.147(6.4)	0.142(7.5)	0.544(18.)	0.851(11.)	(11.1)
Cyl. # 2	0.798(18.)	0.010(16.)	0.170(14.)	0.169(15.)	0.146(6.6)	0.849(18.)	(14.8)
Cyl. # 3	0.969(7.2)	0.016(36.)	0.183(6.3)	0.166(7.1)	0.088(15.)	**0.980**(6.7)	(13.3)
Cyl. # 4	0.627(4.5)	0.495(3.5)	0.163(11.)	0.158(11.)	0.601(5.7)	0.711(4.6)	(6.82)

Average of Total Dev.(Excluding Normal) = **15.6%** (**11.5%**), Datapoints Used = **256**

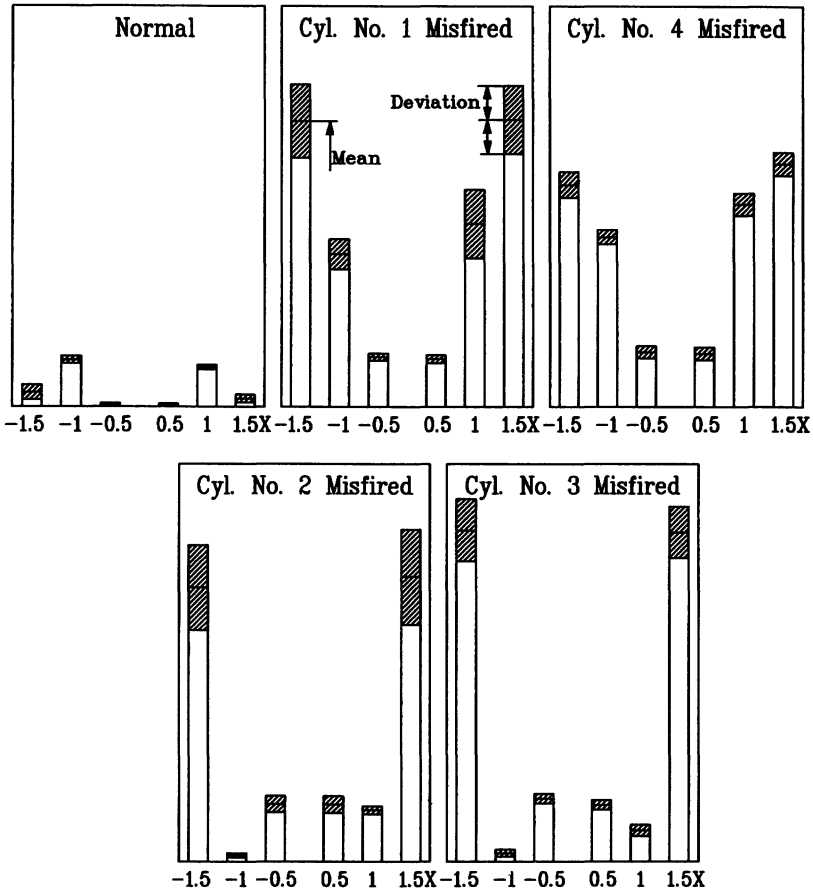

FIGURE 7 Typical dPS estimates by FFT: compression ignition engine.

Table 3. Percentages of Misclassification (ML/FFT): Compression Ignition Engine at 770 rpm

Patterns Used	N. N. Architectures	No. of Iterations	Percentages of Misclassification (%)				
			Normal	Cyl. #1	Cyl. #2	Cyl. #3	Cyl. #4
P_{pp}	6-5-5	1400/1820	0.0/0.0	0.0/10.0	0.0/0.0	0.0/0.0	0.0/0.0
P_{yy}, P_{zz}	6-5-5	5320/5082	0.0/0.0	20.0/16.7	10.0/13.3	3.3/6.7	0.0/0.0
P_{yy}	3-5-5	6566/6321	0.0/0.0	33.3/26.7	0.0/0.0	3.3/0.0	3.3/13.3
P_{zz}	3-5-5	6916/7063	0.0/0.0	30.0/23.3	13.3/6.7	10.0/20.0	0.0/0.0
$\alpha = 0.8$, $\eta = 0.95$, Limit of RMS Error = 0.005							

Table 4. Percentages of Misclassification (ML/FFT): Spark Ignition Engine at 1500 rpm

Patterns Used	N. N. Architectures	No. of Iterations	Percentages of Misclassification (%)				
			Normal	Cyl. #1	Cyl. #2	Cyl. #3	Cyl. #4
P_{pp}	6-5-5	3087/3647	0.0/0.0	0.0/0.0	0.0/0.0	0.0/0.0	0.0/0.0
P_{yy}, P_{zz}	6-5-5	4046/4165	0.0/0.0	0.0/0.0	0.0/0.0	0.0/0.0	0.0/10.0
P_{yy}	3-5-5	16359/19684	0.0/40.0	10.0/30.0	20.0/20.0	50.0/30.0	40.0/70.0
P_{zz}	3-5-5	3689/5593	0.0/0.0	0.0/0.0	0.0/0.0	0.0/0.0	10.0/10.0
$\alpha = 0.7$, $\eta = 0.9$, Limit of RMS Error = 0.005							

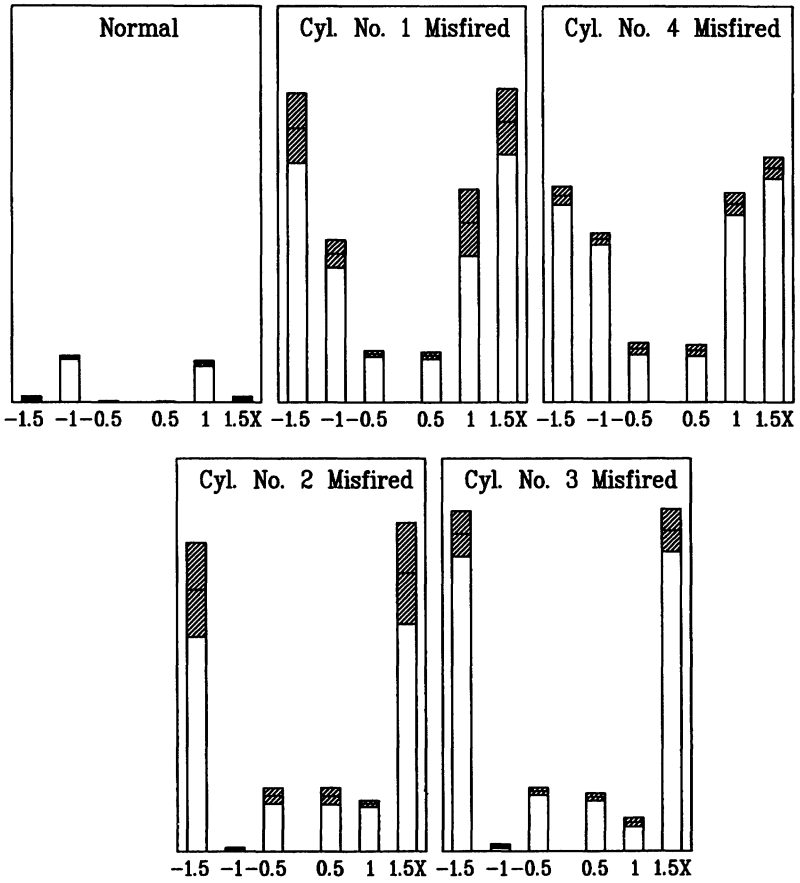

FIGURE 8 Typical dPS estimates by ML: compression ignition engine.

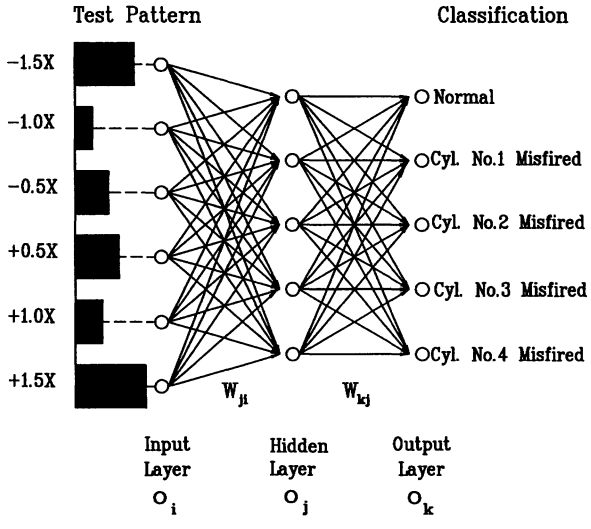

FIGURE 9 Architecture of neural network.

produced as follows:

$$\begin{aligned}
\Delta w_{ji}(l+1) &= \eta \delta_j o_i + \alpha \Delta w_{ji}(l), \\
\Delta w_{kj}(l+1) &= \eta \delta_k o_j + \alpha \Delta w_{kj}(l), \\
\delta_k &= (t_k - o_k) o_k (1 - o_k), \\
\delta_j &= o_j (1 - o_j) \sum_k \delta_k w_{kj}
\end{aligned} \tag{11}$$

where the indices i, j and k denote the input, hidden and output layer nodes, respectively, t_k is the desired output, and o_k and o_j are the actual outputs in each layer. Here α and η are the momentum coefficient and learning rate, respectively. For learning the neural network, three patterns are used in each case of the normal and abnormal conditions: one is the mean of 30 (10) patterns in the compression (spark) ignition engine; the others are patterns with the two largest deviations from the mean. The learning iteration is continued until the rms error of weighting factors is reduced to 0.005, for $\alpha = 0.8$ (0.7) and $\eta = 0.95$ (0.9) in the compression (spark) ignition engine. Figure 10

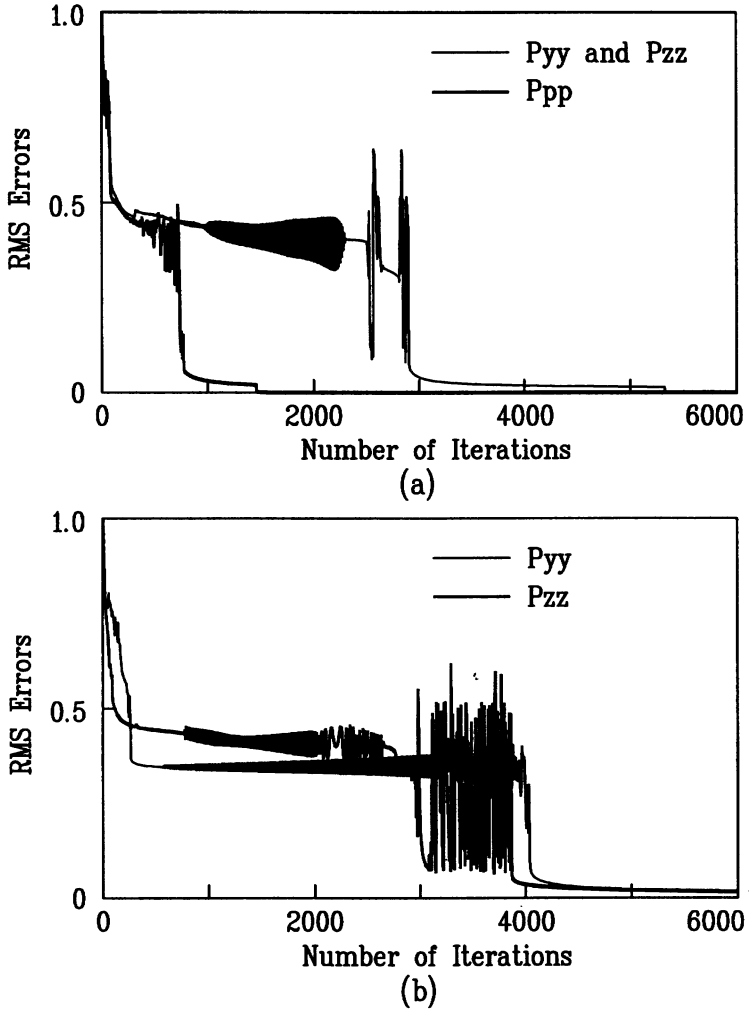

FIGURE 10 Learning curves of neural networks: ML estimates in compression ignition engine.

shows the learning curves for the ML patterns, indicating that it is more effective to use the dPS patterns than the conventional PS patterns on learning the neural network. Tables 3 and 4 present success rates for diagnosis of cylinder power faults along with detection of misfired cylinder position in the compression, resp. spark, ignition engine, indicating that the diagnostic scheme using the dPS is very effective, and far superior to the one using the conventional PS. Here, the ML method shows a similar performance to the FFT method although the number of data points (256) used for the ML method is much less than the number (1024) used for the FFT method.

CONCLUSIONS

A diagnostic method of cylinder power faults utilizing the two-sided directional power spectra of complex-valued vibration signals measured from engine blocks is presented and tested with a compression ignition engine in the laboratory and a vehicle equipped with a spark ignition engine. For the automatic detection/diagnosis of cylinder power faults, a pattern recognition method using the multi-layer neural network is employed. The experimental results show that the diagnostic scheme using the ML estimate of the dPS, which has been originally developed for rotating machine diagnosis, can also be a tool for diagnosis of nonrotating machines such as automobile engines.

ACKNOWLEDGMENT

This research work was supported in part by a grant from the Korea Science and Engineering Foundation.

REFERENCES

Burg, J. P., 1972, "The Relationship between Maximum Entropy Spectra and Maximum Likelihood Spectra," *Geophysics*, Vol. 37(2), pp. 375–376.

Capon, J., 1969, "High Resolution Frequency-Wave Number Spectrum Analysis," *Proceedings of the IEEE*, Vol. 57, pp. 1408–1418.

Connolly, F. T., and Yagle, A. E., 1993, "Modeling and Identification of the Combustion Pressure Process in Internal Combustion Engines: II- Experimental Results," *ASME J. of Engineering for Gas Turbines and Power*, Vol. 115, pp. 801–809.

Foias, C., Frazho, A. E., and Sherman, P. J., 1989, "A Geometric Approach to the Maximum Likelihood Spectral Estimator for Sinusoids in Noise," *IEEE Transaction on Information Theory*, IT-34, pp. 1066–1070.

Kay, S. M., 1988, *Modern Spectral Estimation: Theory and Application*, Prentice Hall.

Kim, J. T., and Lyon, R. H., 1992, "Cepstral Analysis as a Tool for Robust Processing, Deverberation and Detection of Transients," *Mechanical System and Signal Processing*, Vol. 6(1), pp. 1–15.

Lacoss, R. T., 1971, "Data Adaptive Spectral Analysis Methods," *Geophysics*, Vol. 36, pp. 661–675.

Lee, C. W., 1993, *Vibration Analysis of Rotors*, Dordrecht: Kluwer.

Lee, C. W., and Joh, Y. D., 1991, "A New Horizon in Modal Testing of Rotating Machinery, Keynote Paper," *Proceedings of Asia-Pacific Vibration Conference*, Melbourne.

Lee, C. W., and Joh, C. Y., 1994a, "Development of Use of the Directional Frequency Response Functions for Diagnosis of Anisotropy and Asymmetry in Rotating Machinery: Theory," *Mechanical Systems and Signal Processing*, Vol. 8(6), pp. 665–678.

Lee, C. W., and Joh, C. Y., 1994b, "Use of Directional Spectra for Diagnosis of Asymmetry/Anisotropy in Rotor Systems," *Proceedings of the Fourth International Conference on Rotor Dynamics*, Chicago, USA, pp. 97–101.

Pao, Y. H., 1989, *Adaptive Pattern Recognition and Neural Networks*, Addison-Wesley publishing company.

Rizzoni, G., 1989, "Diagnosis of Individual Cylinder Misfires by Signature Analysis of Crankshaft Speed Fluctuations," *SAE 890884*, pp. 1572–1581.

Sherman, P. J., 1991, "Three Techniques for Harmonic Retrieval in Unknown Colored Noise," *Mechanical Systems and Signal Processing*, Vol. 5(3), pp. 183–197.

Sherman, P. J., and Lou, K. N., 1989, "Application of the ML Spectral Estimates for Identification of Defects in Rotating Machinery," *Proceedings of 7th International Conference on Modal Analysis*, Las Vegas, pp. 1587–1590.